Research Square

Preprints are preliminary reports that have not undergone peer review.
They should not be considered conclusive, used to inform clinical practice,
or referenced by the media as validated information.

Performance Analysis of FACTS Devices for Stability and Control of 1100 kV Power System

Mohammad Ali

malixbd@ieee.org

Atlantic International University https://orcid.org/0009-0001-2184-7978

Research Article

Keywords: Flexible ac transmission systems (FACTS), power oscillation damping, SSSC, STATCOM, SVC, TCSC, transient stability, UHV ac transmission, UPFC, voltage stability, wide-area control

Posted Date: November 3rd, 2026

DOI: https://doi.org/10.21203/rs.3.rs-11571739/v1

License: This work is licensed under a Creative Commons Attribution 4.0 International License.
Read Full License

Additional Declarations: The authors declare no competing interests.

Performance Analysis of FACTS Devices for Stability and Control of 1100 kV Power System

Mohammad Ali
School of Science & Engineering, Atlantic International University (AIU)
Honolulu, HI 96813, United States
e-mail: malixbd@ieee.org

***Abstract*—Ultra-high-voltage (UHV) ac corridors rated at 1100 kV carry several gigawatts over hundreds of kilometres, so their usable capacity is limited by angle, voltage and oscillatory stability long before conductor thermal limits are reached. This paper presents a consistent, quantitative performance analysis of five flexible ac transmission system (FACTS) controllers—the static var compensator (SVC), static synchronous compensator (STATCOM), thyristor-controlled series capacitor (TCSC), static synchronous series compensator (SSSC) and unified power flow controller (UPFC)—applied to a 600 km double-circuit 1100 kV corridor that connects a 12 GW generation hub to a receiving grid. The system architecture, colour circuit topologies and mathematical models (distributed-parameter line, flux-decay generator with high-gain static exciter, current- and voltage-injection device models and a wide-area power-oscillation damper with communication latency) are developed and implemented in a phasor-domain simulator. Power–angle and P–V analysis, eigenvalue analysis, time-domain fault simulation with critical clearing time (CCT) search and a latency sensitivity study are performed under identical operating conditions. At a 7 GW transfer the corridor's 0.83 Hz electromechanical mode has only 1.5 % damping; wide-area damping control raises it to about 10 % with ±3 Gvar shunt controllers and to about 20 % with series-connected controllers. The TCSC extends the CCT from 146 ms to 268 ms and the N-1 voltage-stability limit from 4.46 GW to 7.06 GW, whereas the UPFC gives the largest loadability gain (+65 % under N-1) and the best voltage support. The results provide practical guidance for selecting, rating and coordinating FACTS controllers on 1100 kV systems.**

***Index Terms*—Flexible ac transmission systems (FACTS), power oscillation damping, SSSC, STATCOM, SVC, TCSC, transient stability, UHV ac transmission, UPFC, voltage stability, wide-area control.**

I. Introduction

Ultra-high-voltage (UHV) ac transmission at the 1000 kV nominal / 1100 kV maximum-voltage class (U_m = 1100 kV in IEC 60038 [1]) is the backbone of long-distance, bulk-power corridors in which several gigawatts must be moved from remote coal, hydro, nuclear and renewable bases to distant load centres [2], [3]. China's first 1000 kV demonstration line, Jindongnan–Nanyang–Jingmen, entered commercial operation in January 2009 over a route of about 640 km and has since been followed by a meshed UHV ac grid; 1100 kV and 1200 kV class technology has also been developed in Japan and India [2], [3]. Compared with 500 kV and 765 kV networks, an 1100 kV line has a low surge impedance (about 245 Ω for an eight-conductor bundle), a very large charging power (about 5.3 Mvar/km) and a surge-impedance loading (SIL) close to 4.9 GW per circuit.

These properties make the planning problem of an 1100 kV corridor fundamentally a stability problem. With 500–1000 km route lengths, the transmission angle at rated power approaches the steady-state limit, the post-contingency network (one circuit tripped) may not have enough synchronising power to survive a severe fault, the reactive-power balance swings from large surpluses at light load to large deficits at heavy load, and the aggregate generation hub forms a poorly damped electromechanical mode with the receiving grid [4], [5]. According to the IEEE/CIGRE classification [6], [7], rotor-angle (small- and large-disturbance) and voltage stability must therefore be assessed together. IEC TS 63042-101 identifies reactive-power compensation and voltage regulation as core design tasks for UHV ac systems [8].

Flexible ac transmission system (FACTS) controllers address exactly these limitations by controlling, at power-electronic speed, the three parameters of the power-transfer equation—voltage, impedance and angle [9]–[11]. Shunt controllers (SVC and STATCOM) hold the voltage at an intermediate bus and effectively halve the electrical length of the line; series controllers (fixed or thyristor-controlled series capacitors, TCSC, and the converter-based SSSC) cancel part of the line reactance; and the UPFC combines a shunt and a series converter to control voltage, impedance and angle simultaneously [12]–[14]. Supplementary power-oscillation-damping (POD) loops, increasingly fed by synchrophasor measurements from a wide-area measurement system (WAMS), add damping torque to inter-area modes [15]–[17].

A large body of work has compared FACTS controllers—for example, PSS, SVC and STATCOM for oscillation damping [18], SVC and TCSC in voltage collapse [19], and unified Phillips–Heffron models for damping analysis [16]—but most studies use 230–500 kV benchmark systems, different ratings for each device, or a single stability aspect at a time. At 1100 kV, three factors change the picture: the very high charging power interacts with shunt-device sizing, the series devices must be engineered for line-potential platforms and fault currents of 50–63 kA, and the multi-gigawatt power swings make communication latency in wide-area control a practical constraint. A consistent, side-by-side quantitative assessment of all main FACTS families on an 1100 kV corridor is therefore still useful for planners.

This paper provides that assessment. Its contributions are:

- a documented 1100 kV study-system architecture (double-circuit 600 km corridor, mid-point switching station, WAMS layer) with colour circuit diagrams of SVC, STATCOM, TCSC, SSSC and UPFC topologies suitable for 1100 kV application;
- a unified mathematical model—distributed-parameter line, flux-decay generator with IEEE-type static exciter, current- and voltage-injection FACTS models, and a latency-aware POD controller—implemented in a reproducible phasor-domain simulator;
- a like-for-like comparison of the five controllers on power–angle capability, P–V loadability (N-0 and N-1), small-signal damping, critical clearing time, post-fault indices and robustness to WAMS latency;
- practical design guidance for 1100 kV FACTS installations covering connection, insulation, protection, SSR and standards.

Section II describes the system architecture and Section III the controller topologies. Section IV develops the mathematical models and Section V the simulation methodology. Results are discussed in Section VI, practical considerations in Section VII and conclusions are drawn in Section VIII.

II. 1100 kV System Architecture

A. Study System

The study system of Fig. 1 represents a typical point-to-point 1100 kV corridor. A sending-end hub, aggregated as a 12 GW equivalent synchronous machine behind 27/1100 kV generator step-up transformers, feeds the 1100 kV gas-insulated bus S. Two 1100 kV circuits run 300 km to the mid-point switching station M and a further 300 km to the receiving substation R, where 1100/500 kV transformers connect a strong receiving grid represented by its Thevenin equivalent (short-circuit level ≈ 100 GVA, ≈ 52 kA). Each line section is equipped with line-connected shunt reactors at both ends that compensate 80 % of the charging power, a usual practice for UHV lines [2], [8]. A WAMS layer with phasor measurement units (PMUs) at S, M and R, a phasor data concentrator (PDC) compliant with IEEE C37.118.1 [20] and a wide-area damping controller (WADC) supplies the remote speed signal to the FACTS POD loops.

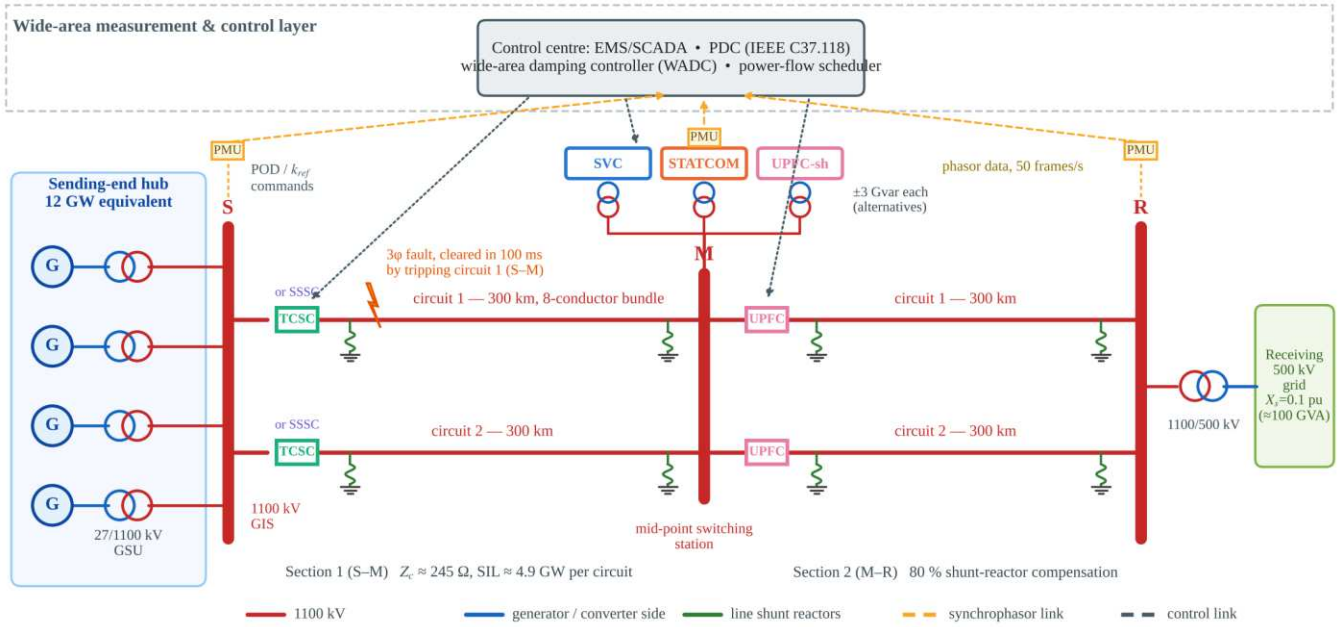


Fig. 1. Architecture of the 1100 kV study system: 12 GW sending hub, 2 × 600 km double-circuit corridor with mid-point switching station, FACTS locations (series devices at S and on section M–R, shunt devices at M), line shunt reactors, fault location and the wide-area measurement and control layer.

Per-unit quantities use S_B = 10 000 MVA and V_B = 1100 kV (Z_B = 121 Ω, I_B = 5.249 kA). The base-case dispatch is 7 GW, i.e. about 70 % of the corridor's natural load (2 × 4.94 GW). The system and machine data are listed in Table I and the line data in Table II. The positive-sequence parameters correspond to an eight-conductor bundle; each 300 km section is represented by its exact equivalent-π circuit (Section IV-A), whose hyperbolic correction is not negligible at βl = 0.322 rad (18.5°).

TABLE I
Generation, Transformer and Receiving-System Data

Quantity	Value
Hub rating / equivalent units	12 000 MVA (12 × 1000 MVA)
Inertia H (own / system base)	4.0 s / 4.8 s
X_d, X'_d (own base)	1.80 pu, 0.30 pu
T'_{d0}, damping D	7.0 s, 3.0 pu
Static exciter K_A, T_A	200, 0.02 s
Field-voltage limits E_{fd}	−4.0 … 5.0 pu
GSU 27/1100 kV reactance	0.14 pu (own base)
Terminal-voltage set point	1.02 pu
Receiving Thevenin X_s	0.10 pu (12.1 Ω)
Base-case transfer P_0	7000 MW (0.70 pu)

System base 10 000 MVA, 1100 kV, 50 Hz.

TABLE II
1100 kV Line Parameters (Per Circuit)

Parameter	Value
r, x per km	0.0080 Ω, 0.263 Ω
b per km (c)	4.38 µS (13.94 nF)
Surge impedance $\|Z_c\|$	245.1 Ω
SIL at 1100 kV	4937 MW
Charging power	5.30 Mvar/km
Section length / sections	300 km / 2
Exact-π series Z′ (300 km)	2.32 + j77.54 Ω
Exact-π shunt B′/2 (300 km)	663 µS (802 Mvar)
Shunt reactor per line end	642 Mvar (80 %)
Total X of one 600 km circuit	155.1 Ω

B. FACTS Placement and Ratings

Shunt controllers are connected at the mid-point bus M, where voltage support is most effective for a symmetrical line [9]. Series controllers (TCSC or SSSC) are installed in each circuit at the sending station S, and the UPFC series converters are inserted at M on section M–R with the shunt converter on bus M. The ratings in Table III were chosen to be representative of practical UHV projects while keeping the comparison fair: all shunt converters are rated ±3000 Mvar (four 750 Mvar valve groups, connected through 1100/66 kV coupling transformers), and all series devices provide 30 % compensation of the 600 km circuit reactance at the 7 GW operating point. The TCSC operates in the capacitive vernier range from 20 % (thyristors blocked) to 50 % (boost factor 2.5), whereas the SSSC and UPFC series converters are limited by their voltage ratings.

TABLE III
FACTS Controller Ratings and Control Parameters

Device	Rating / range	Control
SVC	±3000 Mvar at bus M (TCR–TSC–filters)	slope 3 %, T = 30 ms
STATCOM	±3000 Mvar at bus M (chain-link MMC)	slope 3 %, T = 10 ms
TCSC	X_C = 31.0 Ω per circuit; k = 20–50 % (k_0 = 30 %)	T = 20 ms
SSSC	V_{q0} = 0.135 pu, $\|V_q\| \le$ 0.20 pu per circuit	T = 10 ms
UPFC	±3000 Mvar shunt; series V_{q0} = 0.135 pu, $\|V_0\| \le$ 0.08 pu	T = 10 ms
POD (all)	Δω via PMU, τ = 50 ms	see Table IV

Series ratings are per circuit in per unit of 1100 kV; 1 pu current = 5.25 kA.

C. Hierarchical Control Architecture

The control system follows the four-level hierarchy of Fig. 2. Level 3 schedules FACTS set points from the energy management system and hosts the WADC that converts PMU data into damping commands. Level 2 contains the device controllers—voltage regulators with droop for SVC and STATCOM, compensation-degree controllers for TCSC and SSSC, and the P–Q controller of the UPFC—to which the POD signal is added. Level 1 produces thyristor firing pulses or converter modulation, balances capacitor voltages and runs the inner current loops, while Level 0 comprises the valves, metal-oxide varistors (MOVs), bypass switches and passive components with their fast protection. The separation of time scales (minutes to microseconds) justifies the phasor-domain representation used for Levels 2–3 in this study.

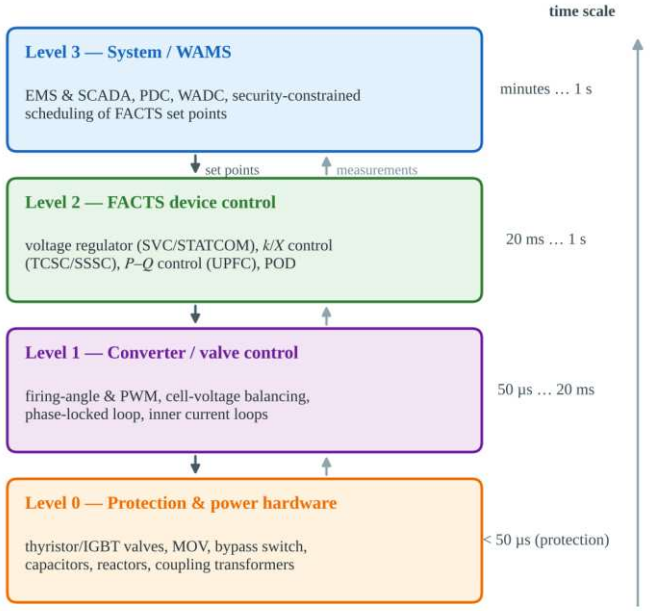


Fig. 2. Hierarchical control architecture of an 1100 kV FACTS installation, from system/WAMS level to valve-level protection, with typical time scales.

III. FACTS Controller Topologies

Figs. 3–7 show the circuit topologies considered, drawn with a common colour code: red for 1100 kV conductors, blue for the converter (medium-voltage) side, purple for power-electronic valves, teal for capacitors, green for reactors and orange for protective and damping elements. Because thyristor and IGBT valves cannot be built economically at 1100 kV phase-to-ground voltage, shunt controllers are connected through dedicated step-down transformers, and series controllers are either placed on insulated platforms at line potential (TCSC) or coupled through series transformers (SSSC, UPFC).

A. Static Var Compensator

The SVC of Fig. 3 combines a thyristor-controlled reactor (TCR), a thyristor-switched capacitor (TSC) and tuned 5th/7th harmonic filters on a 66 kV bus [10], [21]. The TCR is split into two halves around the anti-parallel thyristor valve to limit fault stress on the valve; its fundamental susceptance is varied continuously by the firing angle α, while the TSC is switched at voltage zero-crossing for transient-free insertion. The SVC behaves as a controlled susceptance, so its reactive output falls with the square of the voltage once it reaches its capacitive limit.

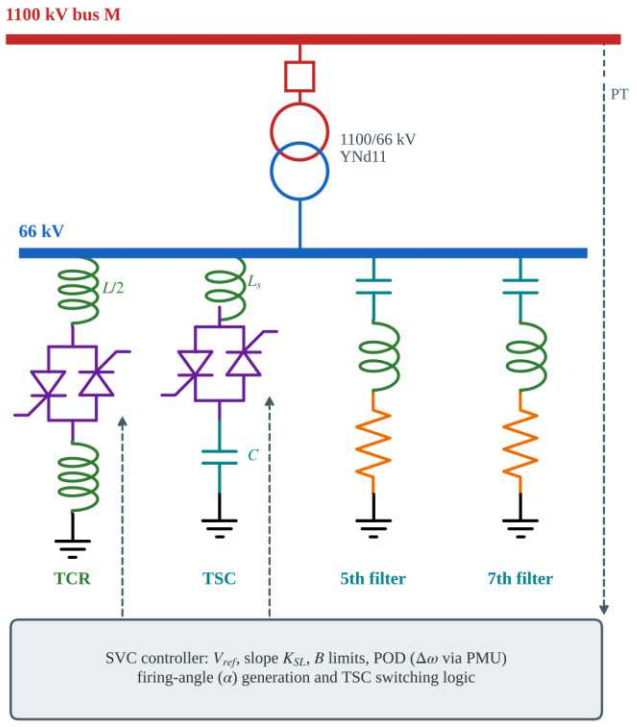


Fig. 3. SVC topology (TCR, TSC and harmonic filters) connected to the 1100 kV mid-point bus through a 1100/66 kV coupling transformer.

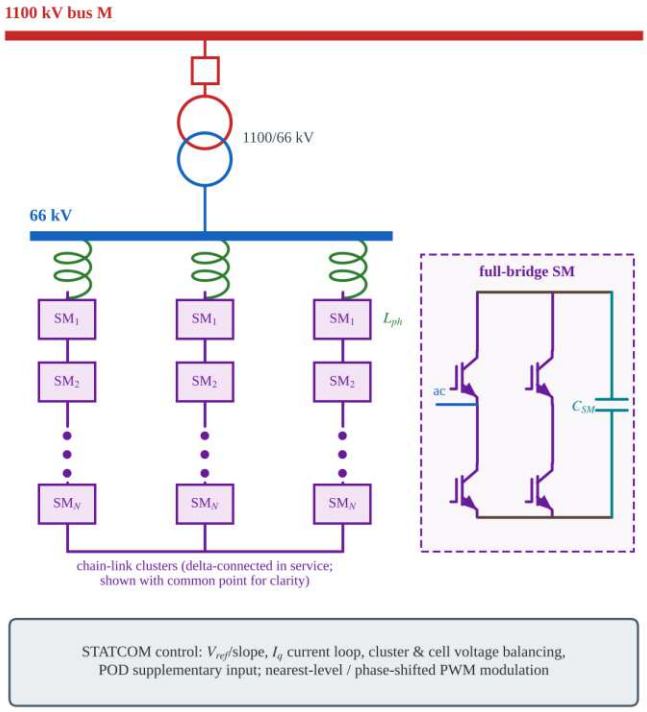


Fig. 4. Chain-link (MMC) STATCOM: phase reactors, delta-connected clusters of full-bridge submodules (detail at right) and converter control functions.

B. Static Synchronous Compensator

The STATCOM of Fig. 4 is a voltage-sourced converter (VSC) of the modular multilevel (chain-link) type [22], [23]. Each delta-connected cluster consists of N series full-bridge submodules (SMs), so the converter synthesises a nearly sinusoidal voltage without large filters. The STATCOM behaves as a controlled current source: its maximum capacitive current is maintained down to low voltage, which is its principal advantage over the SVC during deep voltage dips.

C. Thyristor-Controlled Series Capacitor

The TCSC module of Fig. 5 is a series capacitor C in parallel with a thyristor-controlled reactor L, mounted on an insulated platform at line potential [24]–[26]. An MOV limits the capacitor voltage during line faults; a triggered air gap (TAG) with a damping circuit (L_d, R_d) and a bypass switch protect the MOV against excessive energy. By firing the thyristors before the capacitor-voltage zero crossing, a circulating current boosts the apparent capacitive reactance above X_C (vernier operation), and the TCSC can also be switched to thyristor bypass within one cycle.

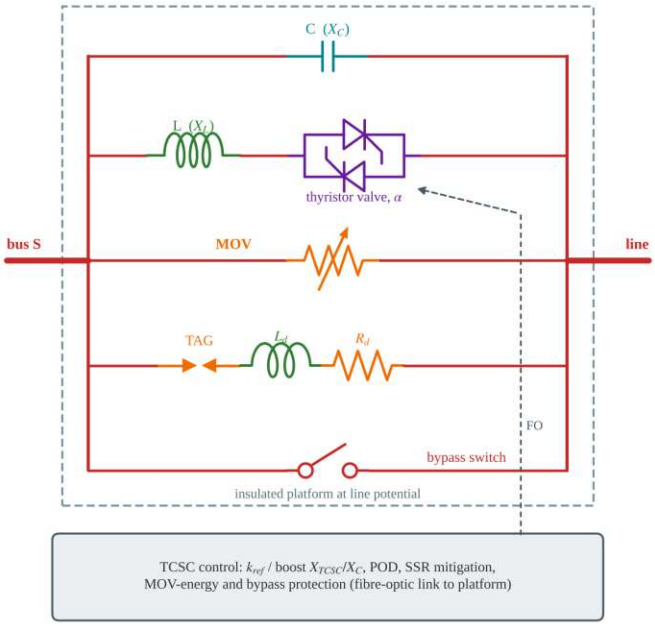


Fig. 5. TCSC module on an insulated platform: capacitor, thyristor-controlled reactor, MOV, triggered air gap with damping circuit and bypass switch.

D. Static Synchronous Series Compensator

The SSSC of Fig. 6 injects a voltage in quadrature with the line current through a series coupling transformer [14]. Because the injected voltage is produced by a VSC rather than by a capacitor, it is independent of the line current, can be either capacitive or inductive, and does not create an electrical resonance with the line inductance—an attractive property where subsynchronous resonance (SSR) with nearby turbine-generators is a concern [27].

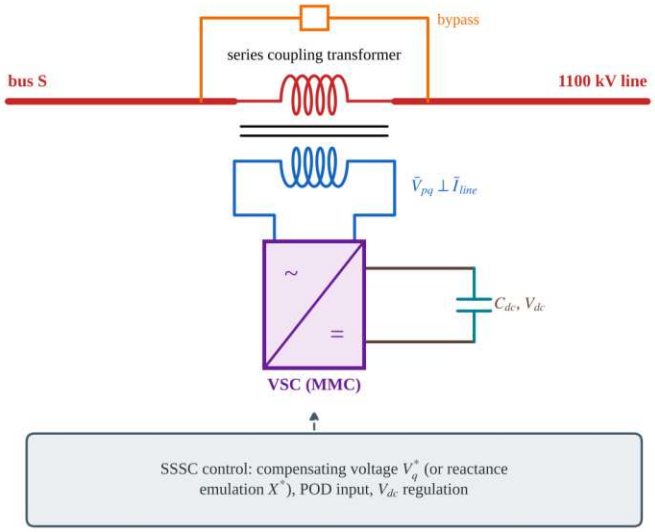


Fig. 6. SSSC: series coupling transformer with bypass, MMC-type VSC and dc capacitor.

E. Unified Power Flow Controller

The UPFC of Fig. 7 couples a shunt VSC and a series VSC through a common dc link [12], [13]. The series converter injects a voltage $\bar{V}_{pq}$ of controllable magnitude and phase; the active power it exchanges with the line is supplied by the shunt converter, which in addition regulates the bus voltage. The UPFC can therefore act as a STATCOM, an SSSC and a phase-shifting transformer at the same time.

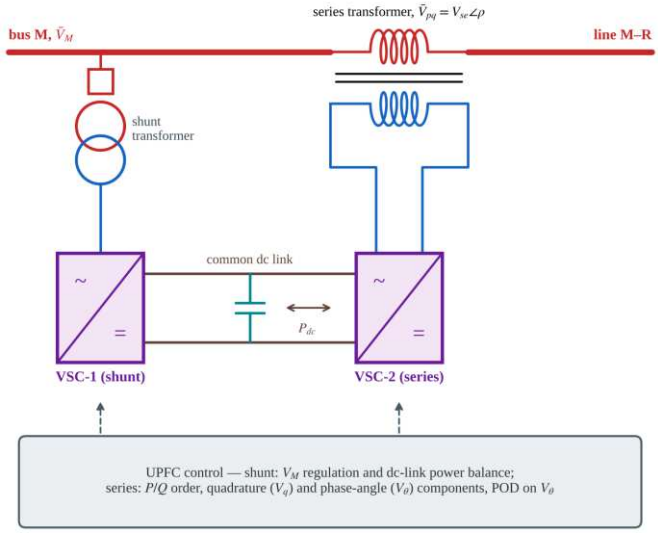


Fig. 7. UPFC: shunt and series VSCs sharing a common dc link, with shunt and series transformers at the mid-point station.

A representative station layout is illustrated in Fig. 8. Its main 1100 kV-specific features are the large air clearances, the single-phase coupling transformers needed for transport limits, and the series-capacitor platform supported by tall post insulators and equipped with its own MOV and valve housing.

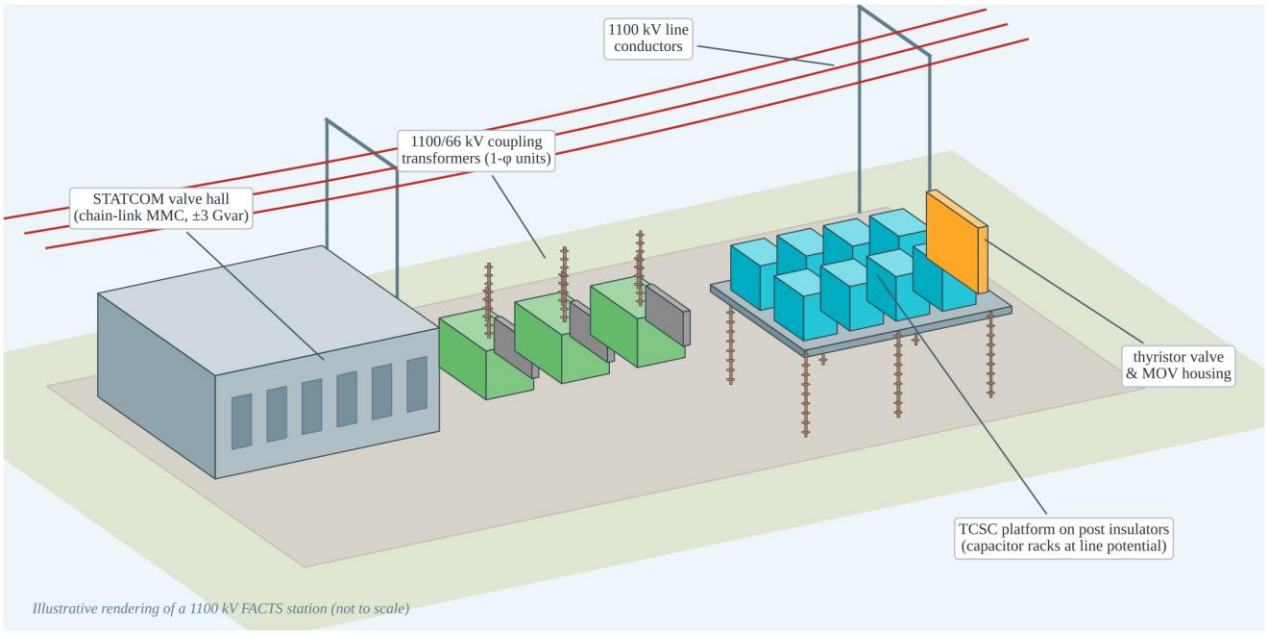


Fig. 8. Illustrative rendering (not to scale) of an 1100 kV FACTS station: STATCOM valve hall, single-phase coupling transformers, TCSC platform on post insulators and 1100 kV line conductors.

IV. Mathematical Models

A. Transmission Line

Each line section of length ℓ is represented by its exact equivalent-π circuit [4]:

$$Z' = Z_c \sinh(\gamma \ell), \qquad \frac{Y'}{2} = \frac{1}{Z_c}\tanh\frac{\gamma\ell}{2} \tag{1}$$

where $Z_c = (z/y)^{1/2}$ and $\gamma = (zy)^{1/2}$ are the surge impedance and propagation constant obtained from the per-kilometre series impedance z = r + jx and shunt admittance y = jb. The natural load is

$$P_{\mathrm{SIL}} = \frac{V^2}{|Z_c|} \tag{2}$$

and the net shunt admittance at each line end, after the line reactor of compensation degree k_{sh}, is

$$Y_{\mathrm{sh}} = \frac{Y'}{2} - j\,k_{\mathrm{sh}}\,\mathrm{Im}\left\{\frac{Y'}{2}\right\} \tag{3}$$

B. Synchronous Generator and Excitation

The aggregate hub is modelled by the flux-decay (one-axis) model with transient saliency neglected ($X'_q = X'_d$) [4], [28]:

$$\dot{\delta} = \omega_b(\omega - 1) \tag{4}$$

$$2H\dot{\omega} = P_m - P_e - D(\omega - 1) \tag{5}$$

$$T'_{d0}\dot{E}'_q = E_{fd} - E'_q - (X_d - X'_d)I_d \tag{6}$$

with $\omega_b = 2\pi\cdot 50$ rad/s. The static exciter is a first-order high-gain system of IEEE Std 421.5 type ST1 structure [29] with output limits:

$$T_A\dot{E}_{fd} = K_A(V_{\mathrm{ref}} - V_t) - E_{fd} \tag{7}$$

The stator algebraic equations and the air-gap power are

$$\bar{V}_t = \bar{E}' - jX'_d\,\bar{I}_g, \qquad P_e = E'_q I_q \tag{8}$$

where I_d and I_q are the components of the generator current in the rotor reference frame defined by δ.

C. Network Solution

The network buses (generator terminal, S, M and R) are described by the nodal equation

$$\mathbf{Y}_{\mathrm{bus}}\,\bar{\mathbf{V}} = \bar{\mathbf{I}}_G + \bar{\mathbf{I}}_\infty + \bar{\mathbf{I}}_F(\bar{\mathbf{V}}, \mathbf{x}) \tag{9}$$

where $\bar{I}_G = \bar{E}'/(jX'_d)$ and $\bar{I}_\infty$ are the Norton injections of the generator and of the receiving system, and $\bar{I}_F$ collects the voltage-dependent FACTS injections. Admittance-type devices (SVC, TCSC) enter Y_{bus} directly; converter-based devices are represented by current injections and solved by a fixed-point iteration inside each function evaluation (tolerance 10^{-12} pu).

D. SVC Model

The fundamental susceptance of the TCR as a function of the firing angle α ($\pi/2 \le \alpha \le \pi$) is [10]

$$B_{\mathrm{TCR}}(\alpha) = \frac{2(\pi - \alpha) + \sin 2\alpha}{\pi X_{\mathrm{TCR}}} \tag{10}$$

At the control level the SVC is a first-order susceptance regulator with droop $K_R = 1/X_{SL}$ and a POD input u_{POD}:

$$T_s\dot{B} = -B + K_R(V_{\mathrm{ref}} - V_M) + u_{\mathrm{POD}}, \qquad Q_{\mathrm{SVC}} = B\,V_M^2 \tag{11}$$

with $B_{\min} \le B \le B_{\max}$. A 3 % slope on the 3000 Mvar device base corresponds to $K_R = 10$ pu on the system base.

E. STATCOM Model

The VSC fundamental voltage $\bar{V}_c = k\ m\ V_{dc}\angle\psi$ (modulation index m, converter constant k) exchanges power with bus M across the phase reactance X_{ph} [9]:

$$P = \frac{V_M V_c}{X_{\mathrm{ph}}}\sin(\theta_M - \psi) \tag{12}$$

$$Q = \frac{V_M[V_M - V_c\cos(\theta_M - \psi)]}{X_{\text{ph}}} \tag{13}$$

For stability studies the converter is represented by its controlled reactive current [30]:

$$T_c\dot{I}_q = -I_q + K_R(V_{\text{ref}} - V_M) + u_{\text{POD}} \tag{14}$$

$$\bar{I}_{\text{ST}} = -jI_q\frac{\bar{V}_M}{V_M}, \qquad Q_{\text{ST}} = I_qV_M, \qquad |I_q| \le I_{\max} \tag{15}$$

Equation (15) shows the key difference from (11): the STATCOM output is proportional to V_{M}, the SVC output to V_{M}^2.

F. TCSC Model

With $\beta = \pi - \alpha$ the steady-state TCSC reactance is [10]

$$X_{\text{TCSC}} = -X_C + C_1[2\beta + \sin 2\beta] - C_2\,\Psi(\beta) \tag{16}$$

$$\Psi(\beta) = \cos^2\beta[\varpi\tan(\varpi\beta) - \tan\beta] \tag{17}$$

where $\varpi = (X_C/X_L)^{1/2}$, $X_{LC} = X_C\,X_L/(X_C - X_L)$, $C_1 = (X_C + X_{LC})/\pi$ and $C_2 = 4X_{LC}^2/(\pi X_L)$. Resonance occurs at $\beta_r = \pi/(2\varpi)$. For the selected module ($X_C = 31.0\ \Omega$, $X_L = 4.59\ \Omega$, $\varpi = 2.6$), $\alpha_r = 145.4°$; boost factors of 1.5 and 2.5 are obtained at $\alpha = 154.8°$ and 150.1°, respectively. The dynamic model uses the compensation degree k as state:

$$T_t\dot{k} = -k + k_0 + u_{\text{POD}}, \qquad X_{SM} = X'_{SM} - k\,X_{L,\text{tot}} \tag{18}$$

where X'_{SM} is the series reactance of the compensated section and $X_{\text{L,tot}}$ that of the whole 600 km circuit. During a fault the TCSC is placed in protective thyristor bypass (k = 0) and reinserted at fault clearing.

G. SSSC Model

The SSSC injects a quadrature voltage that leads the line current $\bar{I}_\ell$ by 90° (capacitive mode):

$$\bar{V}_{pq} = jV_q\frac{\bar{I}_\ell}{|\bar{I}_\ell|}, \qquad T\dot{V}_q = -V_q + V_{q0} + u_{\text{POD}} \tag{19}$$

A series source between buses i and j of a branch with admittance $\bar{y}$ is represented by the equivalent current injections

$$\bar{I}_i = -\bar{y}\,\bar{V}_{pq}, \qquad \bar{I}_j = +\bar{y}\,\bar{V}_{pq} \tag{20}$$

Its equivalent compensation degree, $k_{\text{eq}} = V_q/(X_{\text{L,tot}}\ |\bar{I}_\ell|)$, decreases as the current increases—a property that is important after a circuit is tripped. In the quasi-static (P–V) analysis the slow power-flow scheduler emulates $k_0 = 30$ % up to the 0.20 pu voltage rating.

H. UPFC Model

The series injection of the UPFC has a component in quadrature with the current and a component in quadrature with $\bar{V}_{\text{M}}$ (phase-angle control):

$$\bar{V}_{pq} = jV_q\frac{\bar{I}_\ell}{|\bar{I}_\ell|} + jV_\theta\frac{\bar{V}_M}{V_M} \tag{21}$$

For a lossless dc link the active power of the series converter is supplied by the shunt converter:

$$P_{se} = \text{Re}\{\bar{V}_{pq}\,\text{conj}(\bar{I}_\ell)\} = -P_{sh} \tag{22}$$

$$\bar{I}_{sh} = -\left(jI_q + \frac{P_{se}}{V_M}\right)\frac{\bar{V}_M}{V_M} \tag{23}$$

V_{q} is held at $V_{\text{q0}} = 0.135$ pu (30 % compensation at 7 GW), the POD acts on V_θ, and the shunt current I_{q} regulates V_{M} as in (14).

I. Idealised Power-Transfer Relations

For a lossless line of reactance X between two equal voltages V with angle δ, the classical transfer relations are [9]:

$$P_0 = \frac{V^2}{X}\sin\delta, \qquad V_M = V\cos\frac{\delta}{2} \tag{24}$$

$$P_{\text{sh}} = \frac{2V^2}{X}\sin\frac{\delta}{2} \tag{25}$$

$$P_{\text{ser}} = \frac{V^2}{X(1-k)}\sin\delta \tag{26}$$

$$P_{\text{SSSC}} = \frac{V^2}{X}\sin\delta + \frac{VV_q}{X}\cos\frac{\delta}{2} \tag{27}$$

$$P_{\text{UPFC}} = \frac{V^2}{X}\sin(\delta+\sigma) + \frac{VV_q}{X}\cos\frac{\delta}{2} \tag{28}$$

Equation (25) holds only while the mid-point compensator is within its rating; (26) shows why series compensation raises the whole power–angle curve, and (27)–(28) show the voltage-source character of the SSSC and the additional angle σ of the UPFC. Section VI-C evaluates these relations with finite ratings on the actual 1100 kV network.

J. Power-Oscillation Damping Controller

All devices use the same POD structure (Fig. 9): the generator speed deviation Δω measured by a PMU passes through the WAMS delay, a washout and two identical lead–lag stages [4], [31]:

$$G_{\text{POD}}(s) = K\,\frac{sT_w}{1+sT_w}\left(\frac{1+sT_1}{1+sT_2}\right)^2 e^{-s\tau} \tag{29}$$

The communication delay is represented by a second-order Padé approximation,

$$e^{-s\tau} \approx \frac{1 - s\tau/2 + s^2\tau^2/12}{1 + s\tau/2 + s^2\tau^2/12} \tag{30}$$

and the lead–lag time constants for a total phase compensation φ at the mode frequency ω_{m} follow from

$$\alpha_c = \frac{1+\sin(\varphi/2)}{1-\sin(\varphi/2)}, \quad T_2 = \frac{1}{\omega_m\sqrt{\alpha_c}}, \quad T_1 = \alpha_cT_2 \tag{31}$$

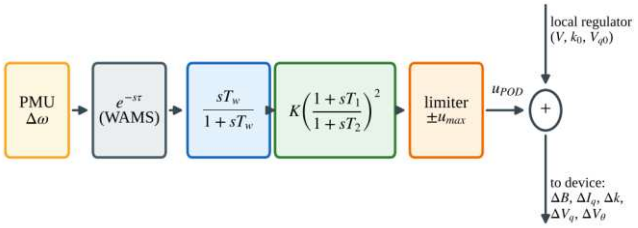


Fig. 9. Wide-area POD controller: PMU speed signal, communication delay, washout, two-stage lead–lag compensator, gain and output limiter.

K. Small-Signal Formulation

The differential–algebraic model $\dot{x} = f(x, y)$, $0 = g(x, y)$ is linearised at the operating point:

$$\Delta\dot{\mathbf{x}} = \mathbf{A}\Delta\mathbf{x}, \quad \mathbf{A} = \mathbf{f}_x - \mathbf{f}_y\,\mathbf{g}_y^{-1}\mathbf{g}_x \tag{32}$$

For each eigenvalue $\lambda_i = \sigma_i \pm j\omega_i$ the damping ratio and frequency are

$$\zeta_i = \frac{-\sigma_i}{\sqrt{\sigma_i^2 + \omega_i^2}}, \qquad f_i = \frac{\omega_i}{2\pi} \tag{33}$$

and the participation of state k in mode i is $p_{ki} = \varphi_{ki}\,\psi_{ik}$, with φ and ψ the right and left eigenvectors [4]. In this work A is obtained by central differences of the reduced model in which the network is solved inside f, which is equivalent to (32).

L. Performance Indices

Transient stability is quantified by the critical clearing time (CCT) and interpreted with the equal-area criterion [4]:

$$\int_{\delta_0}^{\delta_c} (P_m - P_e^{F})\,d\delta = \int_{\delta_c}^{\delta_{\max}} (P_e^{PF} - P_m)\,d\delta \tag{34}$$

where P_e^{F} and P_e^{PF} are the fault-on and post-fault power–angle curves. Post-disturbance damping is measured by the integral of time-weighted absolute speed error,

$$\mathrm{ITAE} = \int_0^{T} t\;|\Delta\omega(t)|\,dt \tag{35}$$

and voltage stability by the maximum loadability $P_{\max}$ of the P–V curve and its relative gain

$$\Delta P_{\max} = \frac{P_{\max}^{\mathrm{FACTS}} - P_{\max}^{\mathrm{base}}}{P_{\max}^{\mathrm{base}}} \times 100\,\% \tag{36}$$

V. Simulation Methodology

The models of Section IV were implemented in a purpose-written phasor-domain (RMS) simulator in Python (NumPy/SciPy). For each case the operating point is found by solving the algebraic and steady-state differential equations with a Newton-type solver (residual < 10^{-8} pu) for the 7 GW dispatch, a generator terminal voltage of 1.02 pu and, for shunt devices, a mid-point voltage reference of 1.0 pu. Time-domain simulations use a fourth-order Runge–Kutta method with a 1 ms step (2 ms for CCT searches); device limits are implemented with anti-windup.

The design disturbance is a bolted three-phase fault on circuit 1 of section S–M at bus S, applied at t = 0.5 s and cleared after 100 ms (five cycles) by tripping that circuit. During the fault the TCSC is in protective bypass and the SSSC and UPFC series converters are bypassed; all devices resume control at clearing. The CCT is determined by bisection with a resolution of 0.3 ms, a case being declared unstable if δ exceeds 180° or $|\Delta\omega|$ exceeds 0.06 pu within 6 s.

P–V curves are traced for the radial corridor of Fig. 1 with bus S held at 1.0 pu and a load of power factor 0.98 lagging at bus R, using a continuation method parameterised by V_R so that the nose and the lower branch are obtained without singularity. Power–angle curves are computed between stiff 1.0 pu sources at S and R with every device at its ratings.

The POD controllers were tuned on the linearised model with τ = 50 ms. For each device the phase compensation φ (−80° to +80°) and gain K were searched to reach a damping ratio of 20 % for the electromechanical mode with the smallest gain, subject to all other modes keeping at least 10 % damping and to a gain ceiling $K_{\max} = u_{\max}/0.002$ (full output at a speed deviation of 0.1 Hz). The resulting parameters are listed in Table IV.

TABLE IV
Tuned POD Parameters (T_w = 5 s, T = 50 ms)

Device	φ (°)	K	T_1 (s)	T_2 (s)	$u_{\max}$
SVC	+40	150.0	0.265	0.130	0.30
STATCOM	+35	150.0	0.253	0.136	0.30
TCSC	+35	25.0	0.230	0.124	0.20
SSSC	+25	13.5	0.233	0.150	0.12
UPFC	+25	13.0	0.229	0.148	0.08

Outputs: ΔB (SVC), ΔI_q (STATCOM), Δk (TCSC), ΔV_q (SSSC), ΔV_0 (UPFC), all in pu.

VI. Results and Discussion

A. Steady-State Operating Point

Table V compares the 7 GW operating points. Without FACTS the internal angle of the hub is 44.1° and the mid-point voltage sags to 0.980 pu. The shunt controllers restore V_M to 0.994 pu with only 577 Mvar, because the residual 20 % line charging already supplies most of the reactive demand at this loading. The series devices reduce the angle by about 8.3° (to 35.8°), i.e. they release roughly one fifth of the angular stability margin. Line losses change little (≈ 98 MW versus 95 MW), confirming that at 1100 kV FACTS are justified by stability rather than by loss reduction.

TABLE V
Steady-State Operating Point at 7 GW

Case	δ_0 (°)	V_S (pu)	V_M (pu)	θ_M (°)	Loss (MW)
No FACTS	44.1	1.005	0.980	17.3	98
SVC	43.7	1.009	0.994	17.0	96
STATCOM	43.7	1.009	0.994	17.0	96
TCSC	35.8	1.012	0.999	16.9	95
SSSC	35.8	1.012	1.000	16.9	95
UPFC	35.7	1.010	0.999	9.0	95

Angles referred to the receiving infinite bus; θ_M for UPFC is the bus angle before the series injection.

B. Device Characteristics

Fig. 10(a) contrasts the V–I characteristics of the two shunt controllers. Inside the control range both follow the 3 % slope; at the capacitive limit the SVC degenerates into a fixed capacitor (I = $B_{\max}$ V), whereas the STATCOM keeps its rated current. At V_M = 0.5 pu the STATCOM therefore delivers twice the SVC current and twice its reactive power (0.50 versus 0.25 of rating). Fig. 10(b) shows the TCSC reactance computed from (16): the inductive and capacitive regions are separated by the parallel resonance at α_r = 145.4°, and the useful capacitive vernier range extends from X_C = 31.0 Ω to 2.5 X_C.

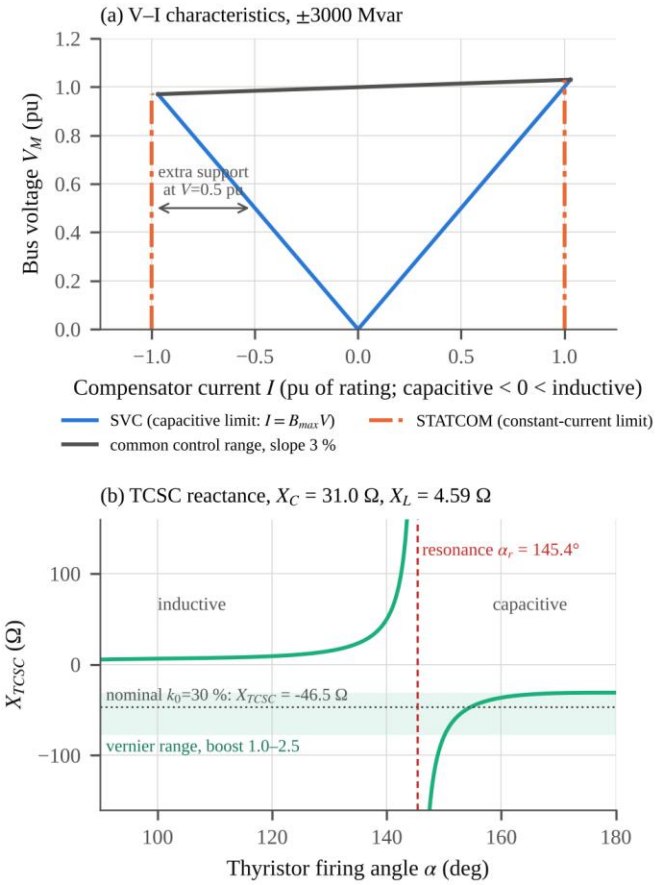


Fig. 10. (a) V–I characteristics of the ±3000 Mvar SVC and STATCOM; (b) TCSC reactance versus firing angle.

C. Power–Angle Capability

Fig. 11 shows the received power as a function of the S–R angle. The intact corridor reaches 15.3 GW at about 88°; the ±3 Gvar shunt devices add only 0.8–1.1 GW because, near the peak, the reactive power required to hold V_M = 1 pu greatly exceeds their rating—an illustration that (25) presupposes unlimited shunt capacity. The TCSC raises the peak to 21.4 GW (+40 %), the SSSC to 17.4 GW and the UPFC to 18.4 GW. With one circuit out (N-1) the base-case peak falls to 10.2 GW while the TCSC case still offers 16.6 GW, because the capacitor in the remaining circuit compensates the same fraction of a now larger reactance.

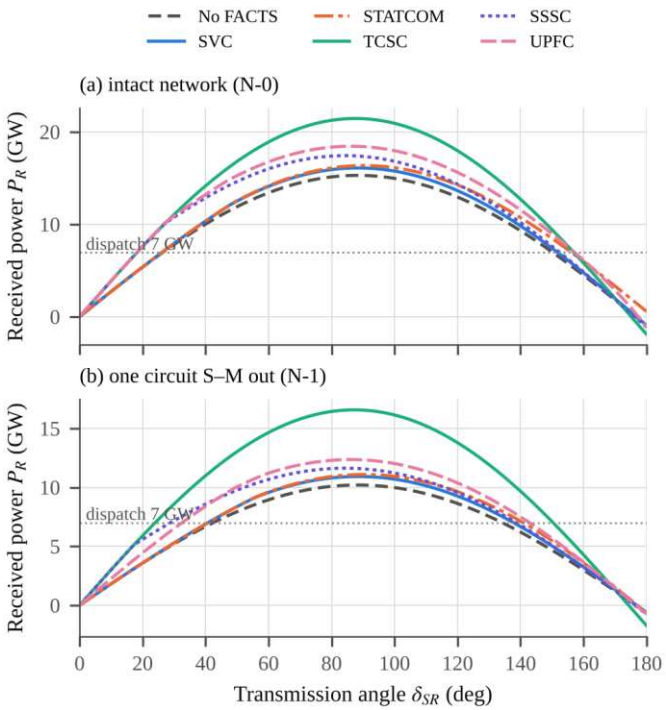


Fig. 11. Power–angle characteristics of the 1100 kV corridor with each FACTS controller: (a) intact network; (b) one circuit of section S–M out of service.

D. Voltage Stability

The P–V curves of Fig. 12 and the loadability limits in Table VI quantify voltage stability. The uncompensated corridor collapses at 6.55 GW (N-0) and 4.46 GW (N-1). Mid-point voltage control by the SVC and STATCOM keeps V_R high until the devices reach their limits and adds 17–19 % (N-0) and 33–38 % (N-1) loadability; the STATCOM is better because its output decreases only linearly with voltage. The series devices shift the nose much further: the TCSC reaches 9.05 GW and 7.06 GW. The SSSC comes close to the TCSC under N-0 (8.51 GW) but loses part of its advantage under N-1 (5.77 GW), because its 0.20 pu voltage rating caps the effective compensation when the full corridor current flows in one circuit. The UPFC, which combines series compensation with mid-point voltage support, gives the highest limits (9.94 GW and 7.37 GW) and keeps V_R above 0.95 pu up to about 7.5 GW in the N-0 case.

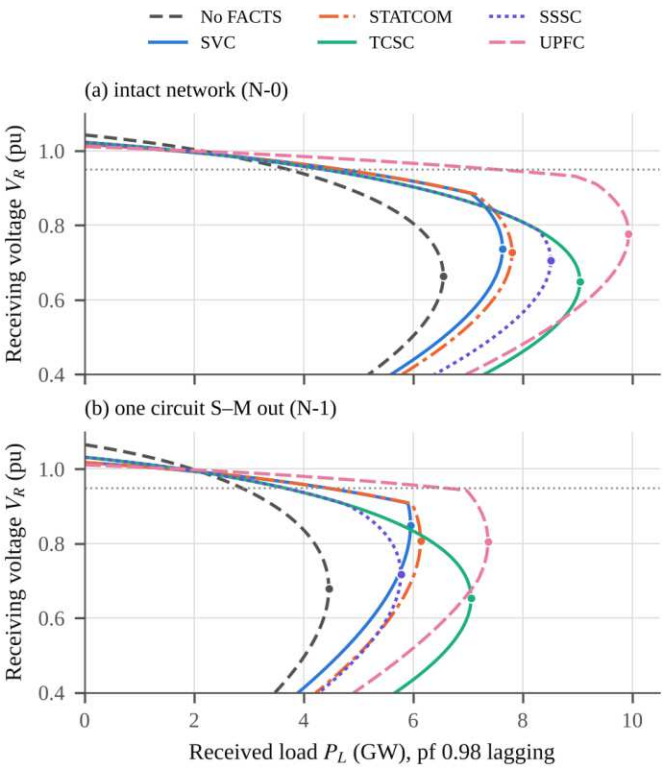


Fig. 12. P–V (nose) curves at the receiving bus R for each controller: (a) intact network; (b) N-1 (one circuit S–M out). Dots mark the maximum loadability.

TABLE VI
MAXIMUM LOADABILITY FROM P–V ANALYSIS

Case	N-0 (GW)	gain (%)	N-1 (GW)	gain (%)
No FACTS	6.55	—	4.46	—
SVC	7.63	+16.5	5.95	+33.5
STATCOM	7.81	+19.2	6.13	+37.6
TCSC	9.05	+38.1	7.06	+58.2
SSSC	8.51	+30.0	5.77	+29.5
UPFC	9.94	+51.7	7.37	+65.2

Load power factor 0.98 lagging; bus S held at 1.0 pu.

E. Small-Signal Stability

The eigenvalues of the electromechanical (EM) mode are listed in Table VII. With the high-gain static exciter the uncompensated corridor has a 0.83 Hz mode with only 1.46 % damping, far below the 5 % planning criterion often used for inter-area modes [5], [32]. The device regulators alone hardly change the damping (1.2–2.0 %); the series devices raise the mode frequency because they stiffen the connection. With the WAMS-POD, the SVC and STATCOM reach 10.0 % and 9.8 % at their gain ceiling, whereas the TCSC, SSSC and UPFC reach the 20 % target with gains well below their ceilings. The root loci of Fig. 13 explain the difference: the controllability of the EM mode from a series device—which modulates the transferred power directly—is several times larger than from a mid-point shunt device, which acts through the voltage sensitivity of the power flow [15], [16]. After the trip of one circuit (post-fault network) the base-case damping is 2.0 %, and the PODs provide 12.6 % (SVC), 31.4 % (TCSC), 17.9 % (SSSC) and 16.5 % (UPFC).

TABLE VII
ELECTROMECHANICAL MODE AT 7 GW (PRE-FAULT NETWORK)

Case	λ without POD	f (Hz)	ζ (%)	λ with POD	ζ (%)
No FACTS	$-0.076 \pm j5.214$	0.830	1.46	—	—
SVC	$-0.103 \pm j5.389$	0.858	1.90	$-0.505 \pm j5.048$	10.0
STATCOM	$-0.107 \pm j5.389$	0.858	1.99	$-0.500 \pm j5.100$	9.8
TCSC	$-0.072 \pm j5.937$	0.945	1.20	$-1.113 \pm j5.358$	20.3
SSSC	$-0.085 \pm j5.355$	0.852	1.59	$-1.043 \pm j4.970$	20.5
UPFC	$-0.109 \pm j5.441$	0.866	2.00	$-1.041 \pm j5.083$	20.1

POD with $\tau = 50$ ms WAMS delay; frequencies with POD are 0.79–0.85 Hz.

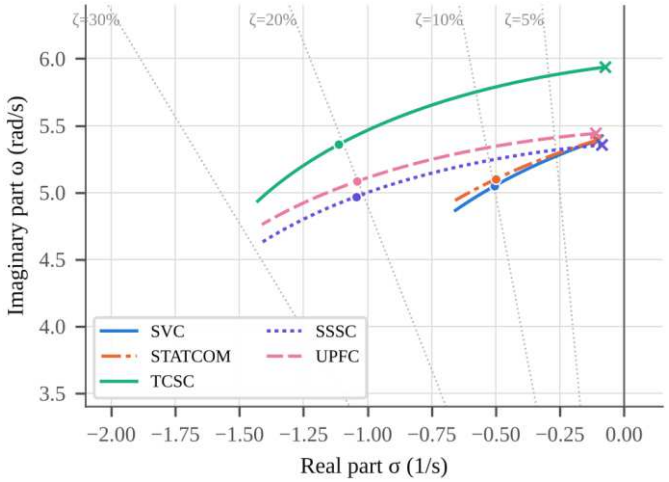


Fig. 13. Root loci of the electromechanical mode as the POD gain increases from 0 (×) to 1.5 times the design gain (dot: design value).

F. Transient Stability

Fig. 14 shows the rotor-angle response to the 100 ms fault. All cases survive the first swing, but the uncompensated system swings to 97.7° and is left with a sustained 0.65 Hz oscillation in the weakened N-1 network. The SVC and STATCOM reduce the first swing by about 10° and damp the oscillation within about 7.5 s. The SSSC and UPFC limit the swing to 77° and 73° and settle in under 4 s; the TCSC, which is boosted to its 50 % limit immediately after reinsertion (Fig. 16(c)), confines the first swing to 54.9° and settles in 1.6 s.

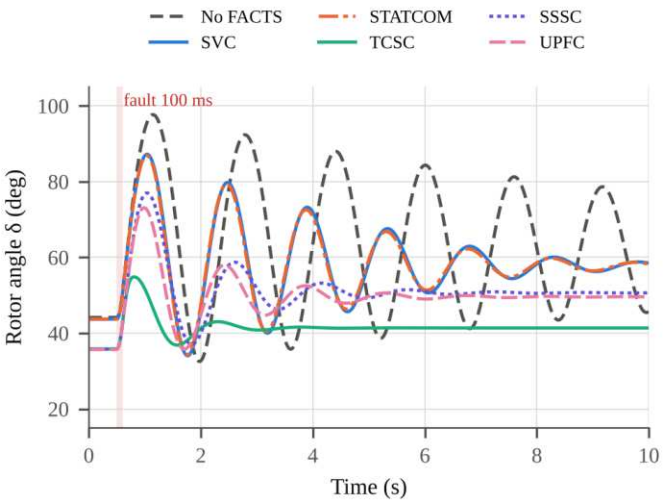


Fig. 14. Rotor angle of the 12 GW hub for a 100 ms three-phase fault at bus S cleared by tripping circuit 1 of section S–M (7 GW transfer, POD active).

Fig. 15 shows the speed deviation and the power delivered by section M–R. The power swings of the uncompensated corridor reach ±1.5 GW at the end of the 10 s window; with the series devices they vanish within about 4 s. Fig. 16 details the mid-point voltage and the device actions. The shunt converters saturate at their 3 Gvar capacitive limit during the first swings, which explains why their POD loops add almost nothing to the CCT. The UPFC keeps V_M above 0.97 pu after clearing, the best voltage performance of all cases, while the SSSC case shows the deepest post-fault dip (0.86 pu) because it lacks shunt support and its injection is limited at high current.

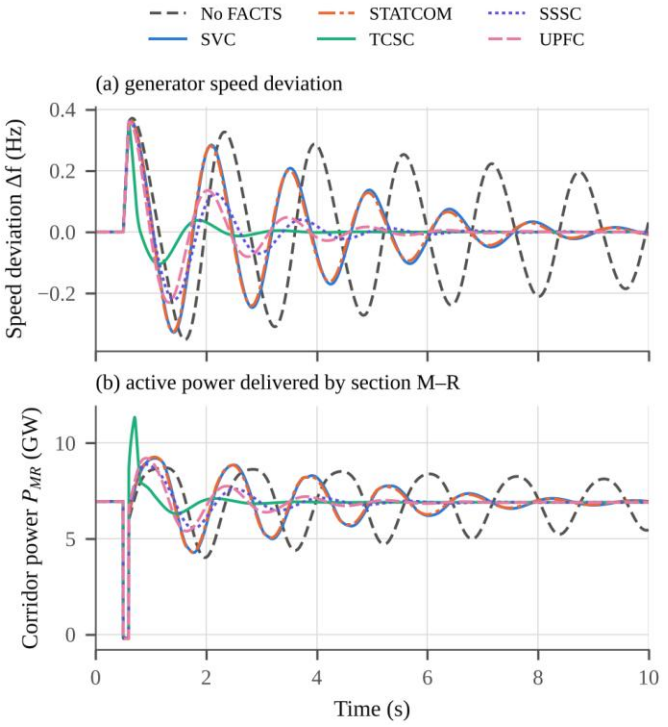


Fig. 15. (a) Generator speed deviation and (b) active power delivered by section M–R for the design fault.

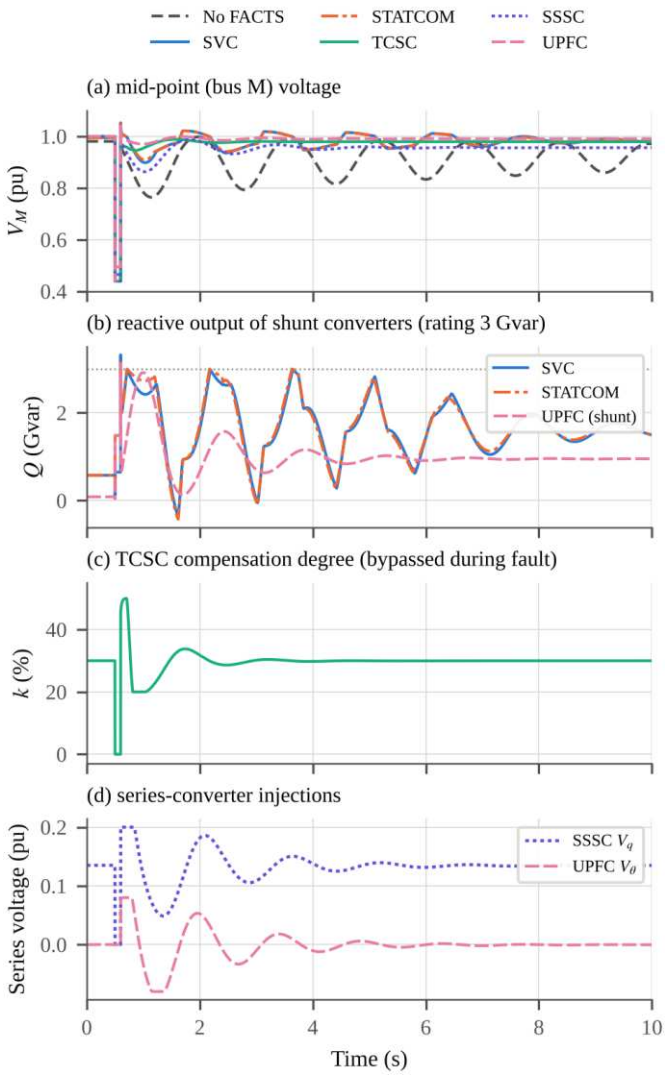


Fig. 16. Mid-point voltage and device actions for the design fault: (a) V_M; (b) reactive output of shunt converters; (c) TCSC compensation degree; (d) SSSC quadrature voltage and UPFC phase-angle component.

TABLE VIII
POST-FAULT PERFORMANCE INDICES (100 MS FAULT, 7 GW, POD ACTIVE)

Case	δ_{max} (°)	$\Delta\delta_1$ (°)	t_s (s)	ITAE ($\times 10^{-3}$)	$V_{M,min}$	CCT (ms)
No FACTS	97.7	53.5	> 9.5	148.0	0.764	146
SVC	87.2	43.5	7.57	55.6	0.898	176
STATCOM	86.9	43.2	7.48	51.9	0.908	184
TCSC	54.9	19.0	1.57	3.1	0.945	268
SSSC	77.0	41.2	3.45	13.7	0.863	188
UPFC	73.1	37.4	3.80	13.5	0.969	210

t_s: last time $|\Delta\omega| > 5 \times 10^{-4}$ pu; $\Delta\delta_1$: first-swing excursion; $V_{M,min}$ after clearing.

The CCT results in Fig. 17 and Table VIII summarise transient stability. At 7 GW the base case tolerates 146 ms, which leaves a margin of only 46 ms over the 100 ms design clearing time. The CCT increases to 176 ms (SVC), 184 ms (STATCOM), 188 ms (SSSC), 210 ms (UPFC) and 268 ms (TCSC). The POD contributes significantly only for the TCSC (232 → 268 ms), whose large modulation range allows the

damping signal to act as a discontinuous boost during the first swing. Fig. 17(b) shows that the base case loses first-swing stability for the 100 ms clearing time above about 7.6 GW; the SVC, STATCOM and SSSC raise this transfer limit to about 8.2–8.5 GW, the UPFC to 9 GW and the TCSC beyond 9 GW (CCT = 180 ms at 9 GW).

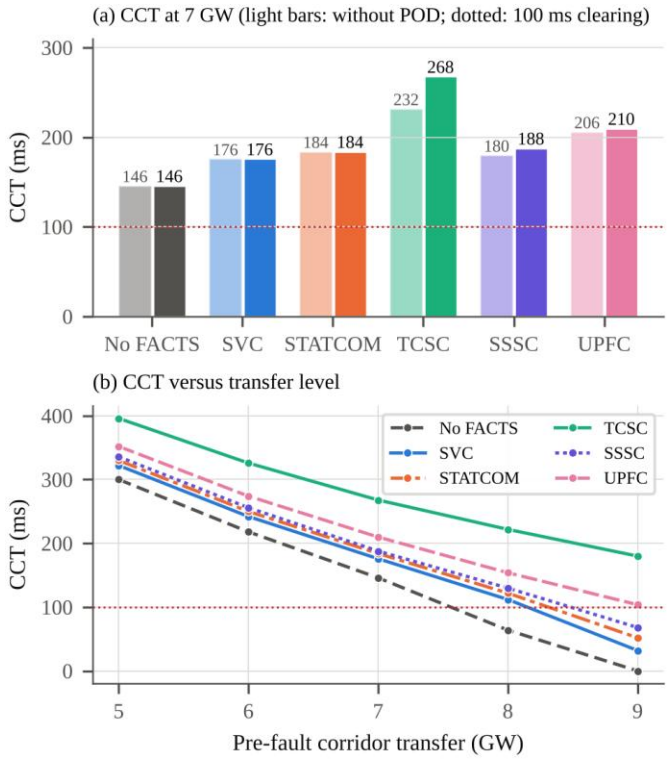


Fig. 17. Critical clearing time: (a) at 7 GW with and without POD; (b) as a function of the pre-fault transfer level (POD active).

TABLE IX
CRITICAL CLEARING TIME (MS) VERSUS TRANSFER LEVEL

Case	5 GW	6 GW	7 GW	8 GW	9 GW
No FACTS	300	218	146	64	0
SVC	322	242	176	112	32
STATCOM	330	250	184	122	52
TCSC	396	326	268	222	180
SSSC	336	256	188	130	68
UPFC	352	274	210	154	104

Bolted three-phase fault at bus S, clearing by tripping circuit 1 of section S–M.

G. Contribution of Wide-Area Damping Control

Fig. 18 isolates the effect of the POD by comparing the corridor power with and without the supplementary loop. Without POD all five devices leave a lightly damped post-fault oscillation (ITAE between 129 × 10^{-3} and 152 × 10^{-3}). With POD the ITAE drops by 60 % (SVC), 98 % (TCSC) and 90 % (UPFC). Hence, for 1100 kV corridors the damping function is not an optional add-on: without it, none of the controllers meets a 5 % damping criterion after the contingency.

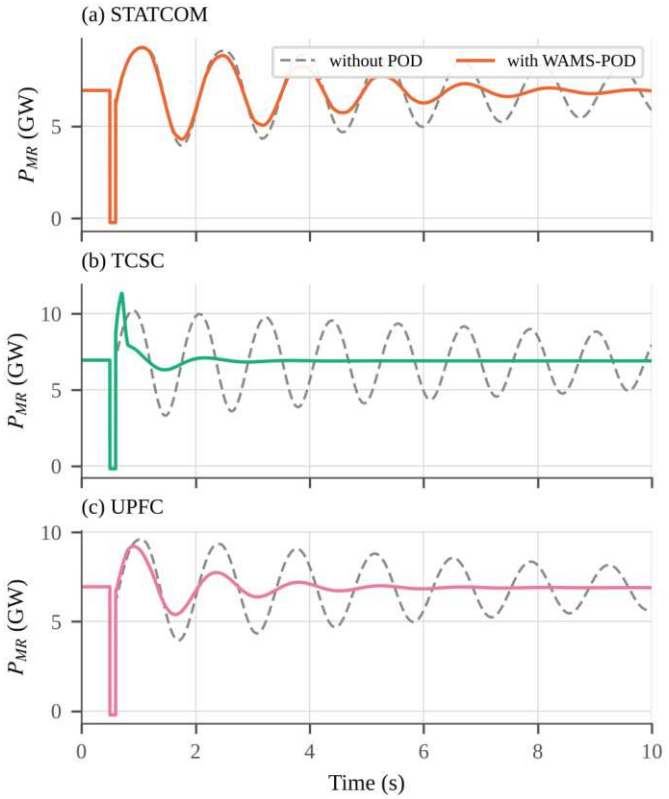


Fig. 18. Power delivered by section M–R with and without WAMS-based POD: (a) STATCOM; (b) TCSC; (c) UPFC.

H. Robustness to Communication Latency

Because the POD uses a remote speed signal, its performance depends on the WAMS round-trip delay. Fig. 19 shows the damping ratio as the delay varies from 0 to 300 ms with the controllers tuned for 50 ms. Moderate additional delay is partly beneficial—it removes some of the excess phase lead—but beyond about 150–180 ms the damping of the series-device loops falls rapidly and drops below 5 % at $\tau \approx 253$ ms (TCSC) and 275 ms (SSSC, UPFC). The shunt-device loops are insensitive to delay but never exceed 14 %. In practice, PMU reporting at 50 frames/s, dedicated optical (OPGW) links and delay-compensated tuning keep the latency of an 1100 kV corridor well below 100 ms, inside the robust region [17], [20].

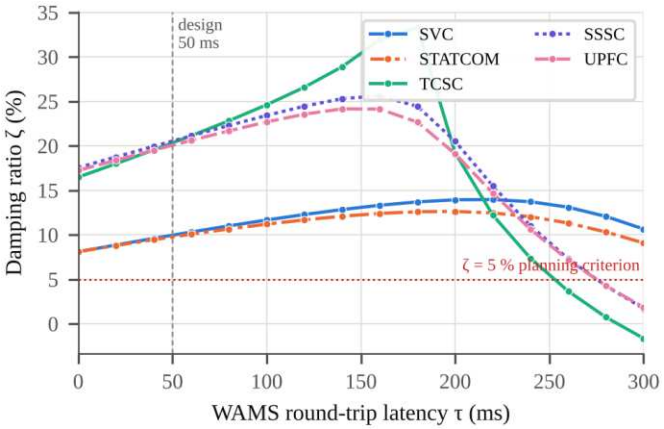


Fig. 19. Damping ratio of the electromechanical mode versus WAMS round-trip latency (controllers tuned for $\tau = 50$ ms).

I. Comparative Assessment

Fig. 20 normalises six computed indices—pre-fault damping, CCT gain, N-1 loadability gain, first-swing reduction, post-fault voltage support and ITAE reduction—to the best performer. The TCSC dominates the angle-stability indices, the UPFC the voltage-related indices, while the SSSC and the two shunt controllers form a middle group. Table X adds the qualitative factors that decide an investment at 1100 kV.

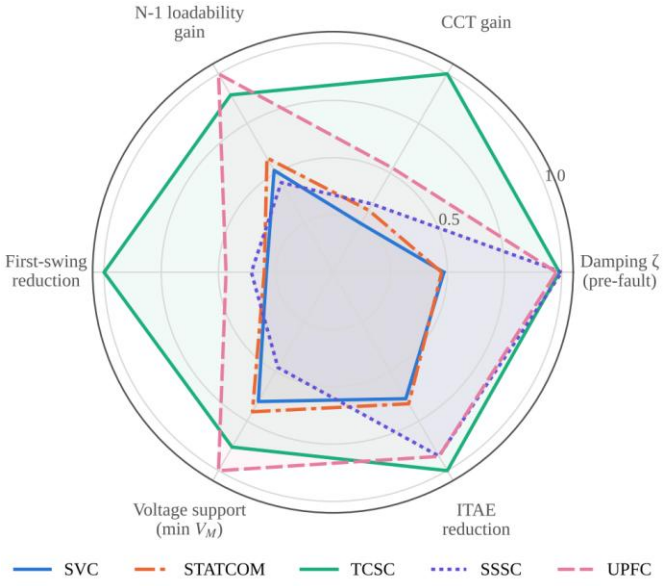


Fig. 20. Normalised comparison of the five FACTS controllers on six computed performance indices (1.0 = best).

TABLE X
QUALITATIVE COMPARISON FOR 1100 KV APPLICATION

Aspect	SVC / STATCOM	TCSC	SSSC	UPFC
Main benefit	voltage, Q reserve	angle stability, damping	damping, flow control	all functions
Output at low V	SVC $\propto I^2$, STATCOM $\propto$ V	n/a	n/a	shunt $\propto$ V
Response	30 / 10 ms	$\approx$ 20 ms	$\approx$ 10 ms	$\approx$ 10 ms
Connection	step-down transformer	platform at line potential	series transformer	shunt + series transformers
SSR risk	none	low (mitigable)	none	none
Fault exposure	low	MOV energy, bypass	converter bypass	converter bypass
Relative cost	low / medium	low–medium	high	highest
UHV service record	in service at UHV	series caps in service	limited	up to 500 kV

Qualitative ranking from this study and [2], [9], [23], [24].

VII. PRACTICAL DESIGN CONSIDERATIONS AT 1100 KV

Connection and rating. FACTS converters are connected to 1100 kV only through transformers (shunt) or insulated platforms and series transformers (series). Shunt devices should be split into several valve groups, each on its own coupling transformer (N-1 redundancy), and coordinated with the switched line reactors so that the fast range of the device is kept free for contingencies; IEC TS 63042-101 gives the reactive-compensation and voltage-regulation framework [8].

Insulation co-ordination. Series-capacitor platforms and series transformers are exposed to switching overvoltages and very fast transients of the UHV network; their insulation must be co-ordinated with the line and substation insulation according to IEC 60071-1 [33] and the device standards [25], [26]. Platform-to-ground insulation, MOV energy and the TAG sparkover level must be specified for the maximum fault current (50–63 kA at 1100 kV).

Line protection and reclosing. Series compensation causes voltage and current inversion and sub-harmonic transients that affect distance protection; adaptive or differential protection and MOV-aware settings are required. Secondary-arc extinction during single-pole auto-reclosing must be checked with the line reactors and neutral reactors in place [2].

Subsynchronous resonance. A fixed capacitor that compensates 30–50 % of a 600 km line can resonate at 15–30 Hz with nearby turbine-generator shafts. TCSC vernier operation makes the device inductive in the subsynchronous range, and the SSSC and UPFC introduce no resonance at all, but screening studies are still needed for thermal and nuclear units at the sending end [27].

Harmonics, testing and standards. Filters and converter topology must keep voltage distortion within IEEE Std 519 [34]. Table XI lists the standards that govern the specification and testing of the devices studied.

TABLE XI
PRINCIPAL STANDARDS FOR 1100 KV FACTS APPLICATIONS

Standard	Scope
IEC 60038:2009	standard voltages; U_m = 1100 kV for UHV
IEC TS 63042-101:2019	UHV ac: voltage regulation, reactive compensation, insulation design
IEC 60071-1:2019	insulation co-ordination
IEEE Std 1031-2011	functional specification of transmission SVCs
IEEE Std 1052-2018	specification of transmission STATCOM systems
IEEE Std 1534-2009	specifying thyristor-controlled series capacitors
IEEE Std 824-2004; IEC 60143-1	series capacitor banks
IEC 61954:2011 / IEC 62927:2017	testing of SVC thyristor valves / STATCOM VSC valves
IEEE Std 421.5-2016	excitation-system models for stability studies
IEEE Std C37.118.1-2011	synchrophasor measurements for WAMS
IEEE Std 519-2014	harmonic control

Limitations of this study. The hub is represented by a single equivalent machine and the receiving grid by a Thevenin source, so intra-area and multi-machine interactions are not captured; the phasor model omits electromagnetic transients, converter switching and unbalanced faults; and SSR is assessed only qualitatively. Detailed EMT studies and multi-machine validation are the natural next steps before an investment decision.

VIII. CONCLUSION

A consistent performance analysis of SVC, STATCOM, TCSC, SSSC and UPFC on a 600 km double-circuit 1100 kV corridor has been presented, including system and control architecture, circuit topologies, mathematical models and a reproducible set of steady-state, small-signal and transient simulations. The main findings are as follows.

- At 7 GW the uncompensated corridor is first-swing stable with a CCT of only 146 ms and has a poorly damped 0.83 Hz mode (1.5 %); stability, not thermal capacity, limits 1100 kV transfers.
- Series compensation is the most effective means for angle stability: the TCSC raises the CCT to 268 ms, the N-0 power–angle peak by 40 % and the N-1 loadability to 7.06 GW.
- The UPFC offers the best combined performance—highest loadability (9.94 GW N-0, 7.37 GW N-1), best post-fault voltage ($V_M \geq 0.97$ pu) and 20 % damping—at the highest cost and complexity.
- ±3 Gvar shunt controllers improve voltage stability by 33–38 % (N-1) but provide only about 10 % damping; the STATCOM outperforms the SVC mainly at depressed voltage.
- Wide-area POD is essential: it raises the damping of the series devices from 1–2 % to 20 % and keeps it above 5 % for WAMS round-trip latencies up to about 250 ms, five times the 50 ms design value.

For new 1100 kV corridors, the results support a combination of controllable series compensation (TCSC, or SSSC/UPFC where flow control or SSR immunity is required) with mid-point STATCOM support, coordinated through a latency-aware wide-area damping controller. Future work will extend the analysis to multi-machine UHV grids, EMT validation of converter controls and coordinated optimisation of FACTS ratings.

REFERENCES

[1] IEC Standard Voltages, IEC 60038:2009, 2009.

[2] Z. Liu, *Ultra-High Voltage AC/DC Grids*. Waltham, MA, USA: Academic Press, 2015.

[3] Y. Shu and W. Chen, "Research and application of UHV power transmission in China," *High Voltage*, vol. 3, no. 1, pp. 1–13, Mar. 2018.

[4] P. Kundur, *Power System Stability and Control*. New York, NY, USA: McGraw-Hill, 1994.

[5] M. Klein, G. J. Rogers, and P. Kundur, "A fundamental study of inter-area oscillations in power systems," *IEEE Trans. Power Syst.*, vol. 6, no. 3, pp. 914–921, Aug. 1991.

[6] P. Kundur *et al.*, "Definition and classification of power system stability," *IEEE Trans. Power Syst.*, vol. 19, no. 3, pp. 1387–1401, Aug. 2004.

[7] N. Hatziargyriou *et al.*, "Definition and classification of power system stability – Revisited & extended," *IEEE Trans. Power Syst.*, vol. 36, no. 4, pp. 3271–3281, Jul. 2021.

[8] UHV AC Transmission Systems – Part 101: Voltage Regulation and Insulation Design, IEC TS 63042-101:2019, 2019.

[9] N. G. Hingorani and L. Gyugyi, *Understanding FACTS: Concepts and Technology of Flexible AC Transmission Systems*. New York, NY, USA: IEEE Press, 2000.

[10] R. M. Mathur and R. K. Varma, *Thyristor-Based FACTS Controllers for Electrical Transmission Systems*. Piscataway, NJ, USA: IEEE Press/Wiley, 2002.

[11] Y. H. Song and A. T. Johns, Eds., *Flexible AC Transmission Systems (FACTS)*. London, U.K.: IEE, 1999.

[12] L. Gyugyi, "Unified power-flow control concept for flexible AC transmission systems," *IEE Proc. C, Gener. Transm. Distrib.*, vol. 139, no. 4, pp. 323–331, Jul. 1992.

[13] L. Gyugyi, C. D. Schauder, S. L. Williams, T. R. Rietman, D. R. Torgerson, and A. Edris, "The unified power flow controller: A new approach to power transmission control," *IEEE Trans. Power Del.*, vol. 10, no. 2, pp. 1085–1097, Apr. 1995.

[14] L. Gyugyi, C. D. Schauder, and K. K. Sen, "Static synchronous series compensator: A solid-state approach to the series compensation of transmission lines," *IEEE Trans. Power Del.*, vol. 12, no. 1, pp. 406–417, Jan. 1997.

[15] M. Noroozian and G. Andersson, "Damping of power system oscillations by use of controllable components," *IEEE Trans. Power Del.*, vol. 9, no. 4, pp. 2046–2054, Oct. 1994.

[16] H. F. Wang and F. J. Swift, "A unified model for the analysis of FACTS devices in damping power system oscillations. Part I: Single-machine infinite-bus power systems," *IEEE Trans. Power Del.*, vol. 12, no. 2, pp. 941–946, Apr. 1997.

[17] A. Chakrabortty and P. P. Khargonekar, "Introduction to wide-area control of power systems," in *Proc. Amer. Control Conf.*, Washington, DC, USA, 2013, pp. 6758–6770.

[18] N. Mithulananthan, C. A. Cañizares, J. Reeve, and G. J. Rogers, "Comparison of PSS, SVC, and STATCOM controllers for damping power system oscillations," *IEEE Trans. Power Syst.*, vol. 18, no. 2, pp. 786–792, May 2003.

[19] C. A. Cañizares and Z. T. Faur, "Analysis of SVC and TCSC controllers in voltage collapse," *IEEE Trans. Power Syst.*, vol. 14, no. 1, pp. 158–165, Feb. 1999.

[20] IEEE Standard for Synchrophasor Measurements for Power Systems, IEEE Std C37.118.1-2011, 2011.

[21] IEEE Guide for the Functional Specification of Transmission Static Var Compensators, IEEE Std 1031-2011, 2011.

[22] A. Lesnicar and R. Marquardt, "An innovative modular multilevel converter topology suitable for a wide power range," in *Proc. IEEE Bologna Power Tech Conf.*, Bologna, Italy, 2003.

[23] IEEE Guide for Specification of Transmission Static Synchronous Compensator (STATCOM) Systems, IEEE Std 1052-2018, 2019.

[24] IEEE Recommended Practice for Specifying Thyristor-Controlled Series Capacitors, IEEE Std 1534-2009, 2009.

[25] IEEE Standard for Series Capacitor Banks in Power Systems, IEEE Std 824-2004, 2004.

[26] Series Capacitors for Power Systems – Part 1: General, IEC 60143-1:2015, 2015.

[27] K. R. Padiyar, *Analysis of Subsynchronous Resonance in Power Systems*. Boston, MA, USA: Kluwer, 1999.

[28] P. W. Sauer and M. A. Pai, *Power System Dynamics and Stability*. Upper Saddle River, NJ, USA: Prentice-Hall, 1998.

[29] IEEE Recommended Practice for Excitation System Models for Power System Stability Studies, IEEE Std 421.5-2016, 2016.

[30] CIGRE Task Force 38.01.08, "Modeling of power electronics equipment (FACTS) in load flow and stability programs: A representation guide for power system planning and analysis," CIGRE Tech. Brochure 145, 1999.

[31] B. Pal and B. Chaudhuri, *Robust Control in Power Systems*. New York, NY, USA: Springer, 2005.

[32] G. Rogers, *Power System Oscillations*. Boston, MA, USA: Kluwer, 2000.

[33] Insulation Co-ordination – Part 1: Definitions, Principles and Rules, IEC 60071-1:2019, 2019.

[34] IEEE Standard for Harmonic Control in Electric Power Systems, IEEE Std 519-2014, 2014.